学士学位论文

Determining magnitudes of large earthquakes in Japan and Alaska using back-projection and P wave amplitudes

学　　号：　**20141000571**

论 文 作 者：　姚　强

学 科 专 业：　地质学

指 导 老 师：　王 墩　教授

培 养 单 位：　地球科学学院

二〇一八年六月

中国地质大学（武汉）学士学位论文原创性声明

本人郑重声明：本人所呈交的学士学位论文《Determining magnitudes of large earthquakes in Japan and Alaska using back-projection and P wave amplitudes》，是本人在指导老师的指导下，在中国地质大学（武汉）攻读学士学位期间独立进行研究工作所取得的成果。论文中除已注明部分外不包含他人已发表或撰写过的研究成果，对论文的完成提供过帮助的有关人员已在文中说明并致以谢意。

本人所呈交的学士学位论文没有违反学术道德和学术规范，没有侵权行为，并愿意承担由此而产生的法律责任和法律后果。

学位论文作者签名：

日期：　　年　　月　　日

摘 要

根据震级可以近似地预估地震能量、断层长度、地震破坏程度、社会影响等[*龙锋等*, 2006]。目前应用比较广泛的震级主要有M_L、M_S、m_b和M_W四种类型。其中前三种震级由于基于较高频的地震波信号，对较大地震震级饱和。也就是说，对超过6.2、7.0和8.5级的大震，得到的m_b、M_L和M_S震级将明显低估真实地震大小。M_W是目前广泛应用、且最为可靠的震级标度（尤其是基于W-phase波形反演更加稳定）。其基于地震断层的破裂长度、面积及平均位错量等静态震源参数，直接对应断层破裂的物理过程，不存在震级饱和现象，一般在震后20到30分钟内可以较为准确地测定地震震级[*陈运泰&刘瑞丰*, 2004; *杨智娴&张培震*, 1998]。但目前基于W-phase波形反演技术有两个需要进一步论证的问题: ① 目前反演所采用的波形数据，其时窗长度是固定的，这对具有较长的震源持续时间的地震，会造成较大误差; ② 该方法因为涉及到低频波反演，要求观测台站具有较好的方位覆盖范围。

所以，快速准确测定大震震级的研究还有很大进步空间和紧迫的社会需求[*倪四道*, 2008]，台阵技术在近年来得到广泛发展和应用，特别是在研究大震震源过程及余震探测方面，加深了对震源破裂展布、破裂能量辐射的频带特征等一系列科学问题的研究[*杜海林&许力生*, 2012]。*Wang et al.* [2017] 借鉴日本建筑研究所 Hara Tatsuhiko 的工作 [*Hara*, 2007; 2008; 2011], 引入全球宽频带地震台记录的直达P波的最大位移，与利用台阵技术和反投影方法得到的震源持续时间相结合，初步提出一种新的震级标度 M_{dt}，来快速精确测定大震震级。此方法主要利用全球台站的数据计算P波在垂向位移的最大幅值，再利用地方密集台网的数据，用反投影方法，来计算地震的震源持续时间，最后将两者通过经验公式结合,得出震级。在时间效率上，该方法快于基于全球地震台网数据的W-phase反演震级方法，与基于区域地震台网数据的W-phase反演震级方法相当。因此将新震级标度M_{dt} 与W-phase 反演结果相互验证、综合利用，将能更好地实现快速准确地测定大震震级及地震减灾工作。

本研究首先根据 M_{dt} 的测定方法，用中国密集区域台网和全球台站的数据（中国台和全球台的台站震中距在10度到60度之间），测定了2008年到2016年发生在日本及其周围的11个浅源大地震（USGS[1]震级≥7.0，深度≤60km）的震级。结果显示，震级可以被准确地计算得出，所用时间在震后6到12分钟内(主要依赖

1 USGS: United States Geological Survey (https://www.usgs.gov/)

于地震到台站的距离)。对于2011年 M9.0大地震，在震后6、8、10和12分钟之后得到的结果依次是9.1、9.0、8.8和8.9。本文尝试用地震附近的其他地震的台站矫正来做反投影，最终得到的震源持续时间和用自身的台站矫正所得结果相比，没有出现大的偏差，证明在求持续时间的过程中，不需要准确的地震位置信息，利用先前储存的地震走时矫正信息库，就可以快速得到震级。

因此，本研究提议建立一套自动实时系统，利用中国台和全球台的数据，以及海量的台站矫正信息库，无需地震定位信息，来测定发生在日本及其周边地区的大震震级。这样快速、准确地得到结果后，可以迅速地发布灾难预警，特别是海啸预防和应急救援等方面。

另外，本文对最近（2018年1月23日）发生在美国阿拉斯加湾附近的M7.9地震，利用当地以及阿拉斯加周围地区的台站数据（震中距在8-15度），沿用上述方法测定其震级。首先用较窄的方位角范围限制台站区域，通过反投影方法计算得到震源持续时间，再加上近台以及地方台的数据，求得P波的最大振幅，最后在震后3到5分钟，可以得到的震级在7.86到8.03之间，这个结果非常靠近7.9（USGS和GCMT[1]所测结果）。

这个例子证实了此方法可以利用地方以及区域台，对大地震快速有效地测定震级，所用时间在震后3到5分钟。因此可以将此方法应用于沿海国家及地区，来测定地震大小和预防海啸。

现今，地震预警所用的算法在为地震震级提供快速结果的时候，具有很大的不确定性。发布不正确的警告信息将极大地破坏社会公众对警报系统的信心。考虑到在震后时间之后的几分钟内，就可以获得更精确的震级，而破坏性海啸波到达海岸地区则需要20-30分钟左右。本研究建议，通过更快速准确的方法来确定震级，如基于本地观测的W-phase反演方法和我们的新方法，为海啸预警提供关键信息。所以，本文认为应充分论证、完善改进该方法，基于全球主要地震台阵（如中国、美国、欧洲、日本Hi-net 等）数据，系统评估该方法的可靠性及稳定性，并与W-phase 等方法相结合，服务于全球地震应急及海啸预警工作。

关键词：震级测定，反投影，实时地震学，海啸预警。

1 GCMT: Global Centroid-Moment-Tensor (http://www.globalcmt.org/)

Abstract

Rapid determination of earthquake magnitude is of importance for estimating shaking damages, and tsunami hazards in coastal countries and regions. Fastest estimate of earthquake size would be from some empirical approaches that are frequently used in earthquake early warning. Local (Richter) magnitude M_L, body wave magnitude m_b, surface wave magnitude M_s, and moment magnitude， M_w are four basic magnitude scales commonly used today for measuring earthquake sizes. For M > = 8.0 earthquakes, the former three magnitude scales become saturated, causing severe underestimation of earthquake size. The M_w scale does not become saturated for earthquakes of any size; so it can provide an accurate estimate of the size of a large earthquake. However, estimating M_w requires entire wave trains including P, S, and surface waves, which takes tens of minutes to reach seismic stations at tele−seismic distances. Therefore, there still are a few problems for accurately estimating magnitude of large earthquakes right after large damage earthquakes.

Motivated by the method of Hara [2007], Wang et al., [2017] proposed a robust algorithm to resolve magnitude, M_{dt} and source length of large earthquakes using seismic data recorded by Hi-net dense arrays and global stations. The system could be useful for rapid tsunami estimation, shaking damage prediction, and possible practical implementation of emergency response strategies. Following the method of M_{dt}, the essay determinates the magnitudes by combining the maximum amplitude of the P waveforms and source durations derived from back-projection.

Here the research determines the magnitudes of 11 $M \geq 7.0$ shallow earthquakes that occurred in and around Japan from 2008 to 2016, using seismic data recorded in China and across the globe. The results suggest that the magnitudes can be accurately estimated 3 to 9 min after origin times of the earthquakes, depending on the epicentral distances to seismic stations in China. For the case of the 2011 M9.0 Tohoku, Japan earthquake, the magnitude is estimated as being 9.1, 9.0, 8.8, 8.9 at 6, 8, 10, 12 min after the origin time, respectively. This research uses station corrections derived from nearby earthquakes to perform back-projection. The final source durations don’t show significant variations, demonstrating that the magnitudes can be estimated with the pre-stored database of station corrections without requiring the catalogue information.

Therefore, here I propose to build an automated system for determining magnitude of large earthquakes in and around Japan using real-time seismic data in China and across the globe and a pre-stored database of station corrections, for disaster mitigation right after a damaging earthquake, especially when dealing with the tsunami evacuation and emergency rescue.

The research also estimates the magnitude of the 23 January 2018 M7.9 Alaska earthquake using seismic stations recorded at local to regional distances in Alaska, US. The research determines the source duration from back-projection results derived from the Alaska stations in a relatively compact azimuth range. Then I calculate the maximum P-wave displacements recorded on a wide azimuth range at distances of 8 to 15 degrees. Combining the source duration and the maximum P-wave displacements, I obtain magnitudes of 7.86 - 8.03 for the 23 January 2018 earthquake in 3-5min, which is very close to the M_w7.9 determined by the USGS and GCMT.

The example validates the new approach for determining magnitude of large earthquakes using local to regional stations, and its time efficiency that magnitudes of large earthquakes can be accurately estimated within in 3-5 min after origin times. Therefore further application of this new method would help accurate estimation of size of large earthquakes that occur off shore and might cause tsunami hazards.

Keywords: Magnitude estimate; Back-projection; Real-time seismology; Tsunami warning.

Contents

0. List of Figures

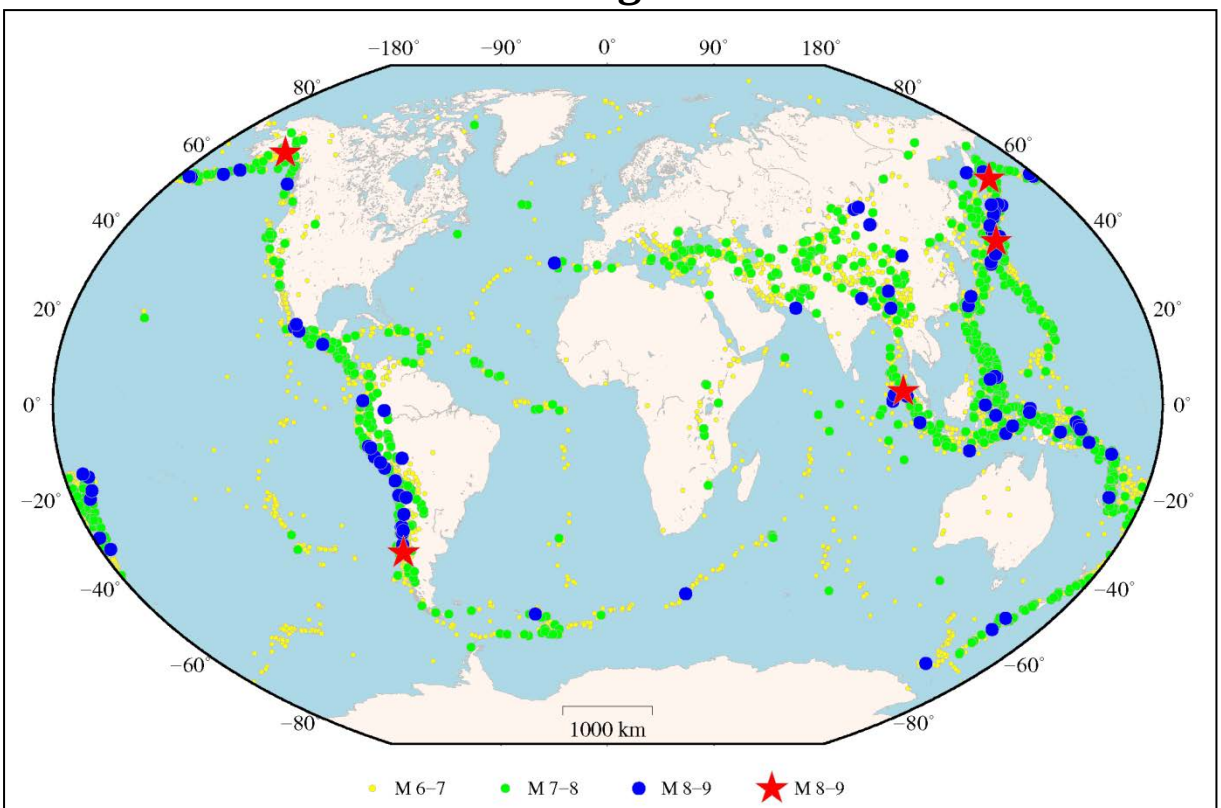

Figure 1.1 Distributions of earthquakes from 1990 to 2018 according to the USGS earthquake catalog. Different colors indicate different magnitudes of earthquakes.

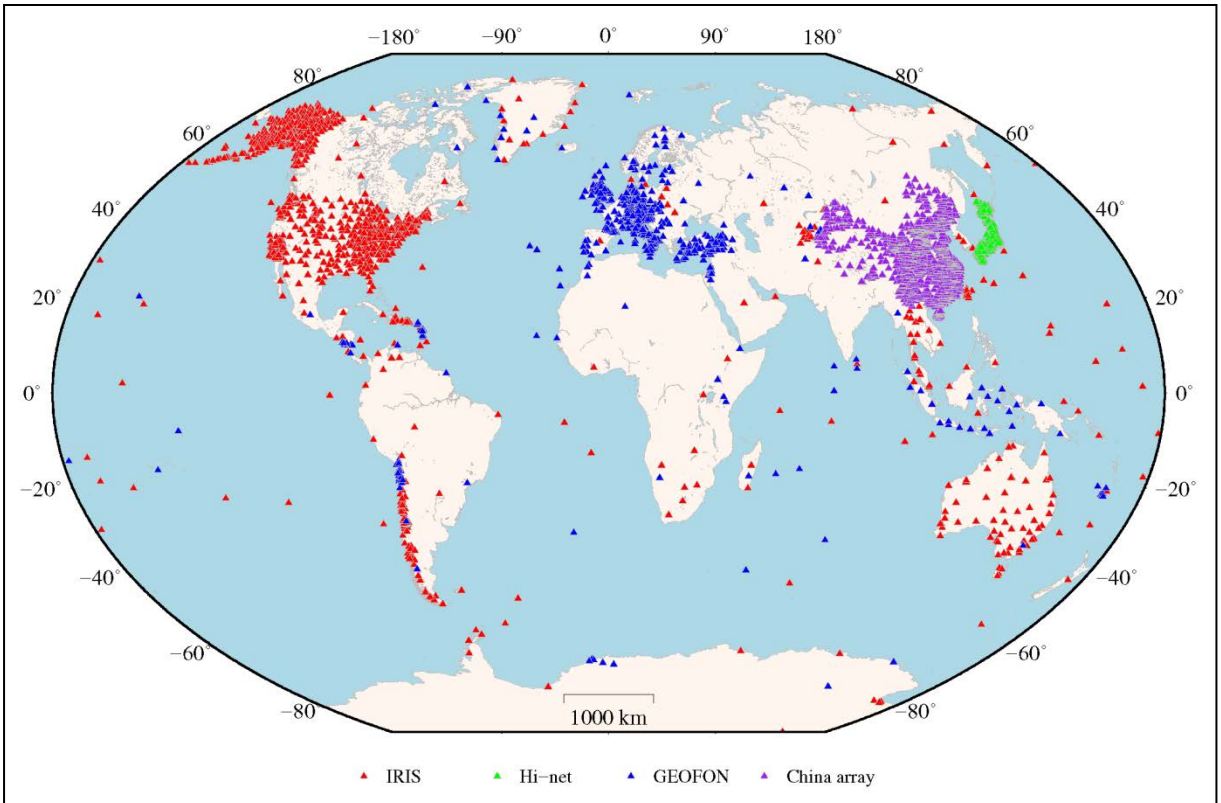

Figure 1.2 Locations of global seismic stations.

Figure 2.1: The maximum displacement of P waveforms. Bottom waveform is seismic wave after removing instrument response of the original waveform (top).
The arriving times of P and S waveforms were labeled by a travel-time software, Taup. The maximum displacement is the larger one between depmax and depmin (absolute value).

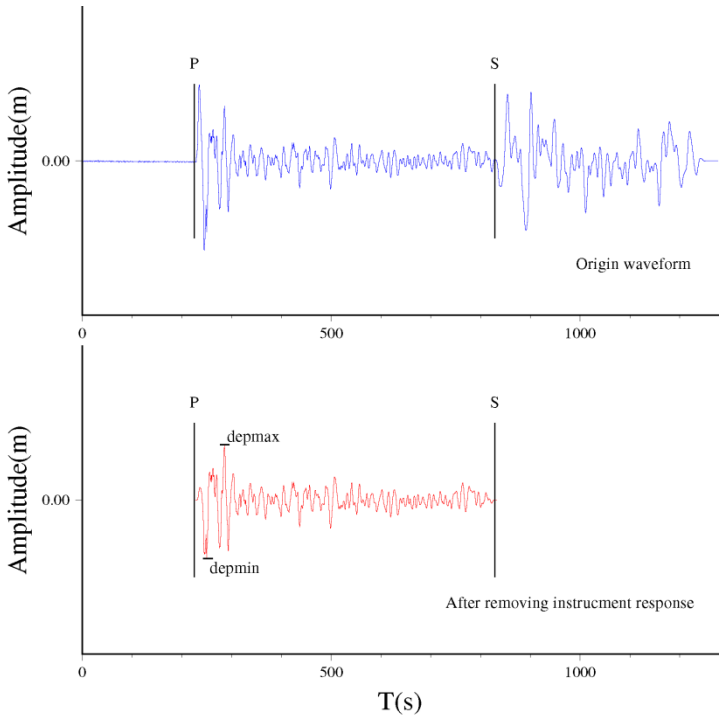

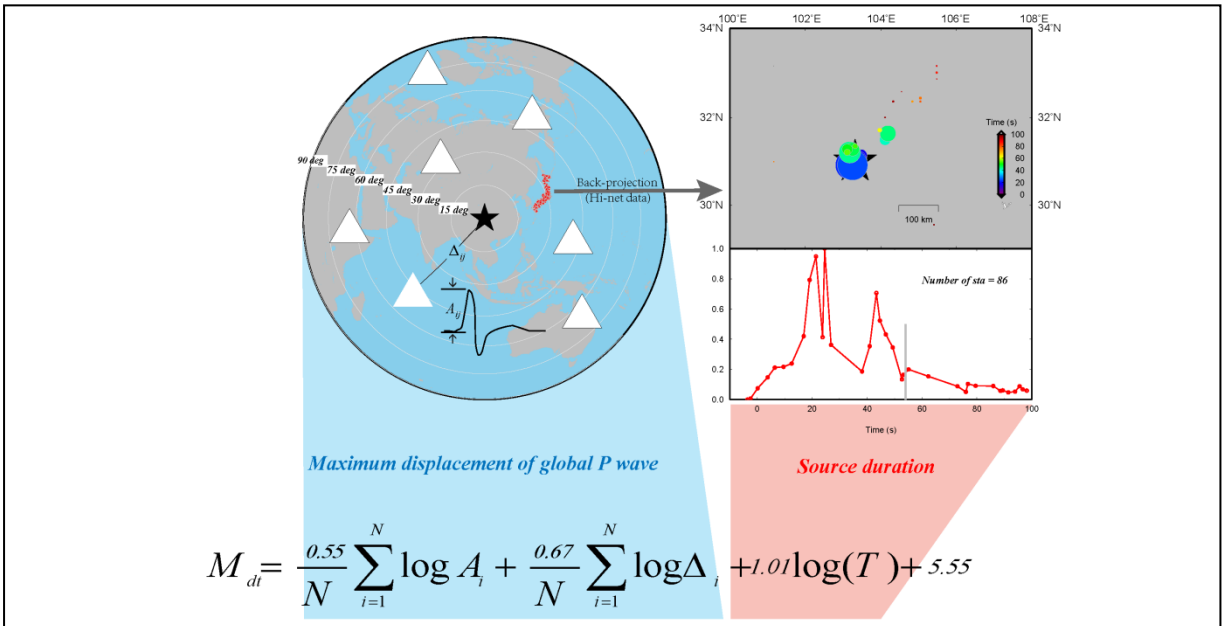

Figure 2.2 Methodology for determining magnitudes of large earthquakes. Magnitude is estimated by combining (left) maximum displacements of global P wave amplitudes and (lower right) source durations. Here the source duration is estimated by back-projection analyses using a large regional seismic array. The grid line in lower right shows the cutoff where the rupture ends. Color circles indicate the local maximums of the stacked energies (upper right). Here A_i is the maximum vertical displacement of the tele-seismic P wave recorded at the i_{th} station, and Δ_i is the epicentral distance (km). Parameter T is the source duration derived from the back-projections, and N is the number of global stations. The operator log denotes the decimal logarithm.

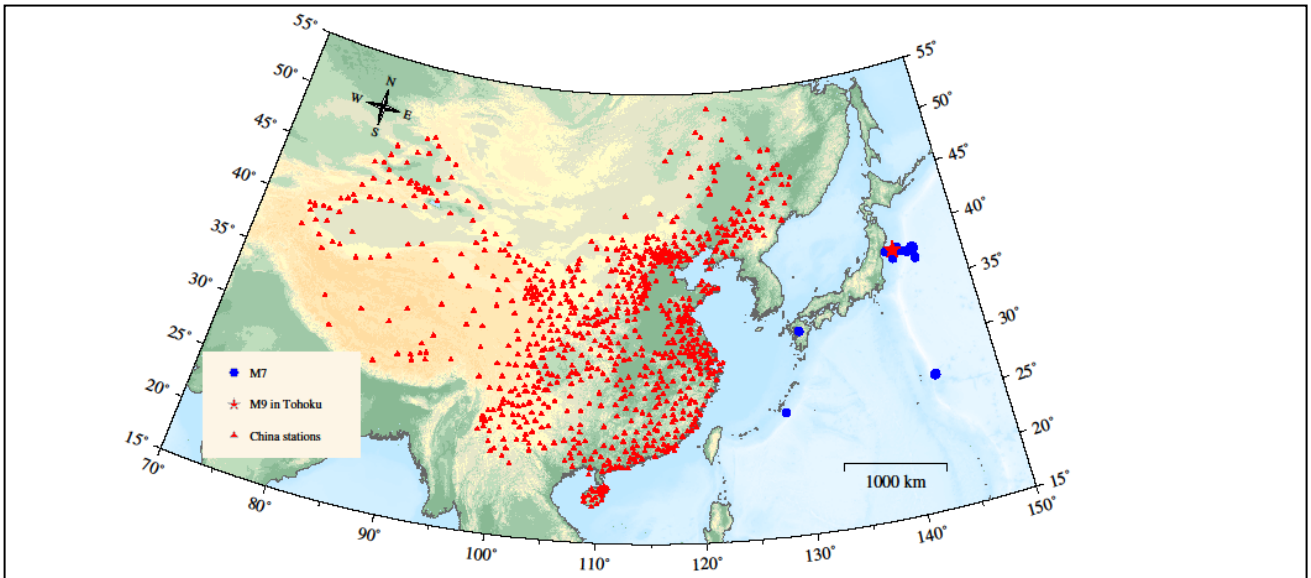

Figure 3.1 Locations of broadband seismic stations in China (red triangle), and earthquakes with M_w larger than or equal to 7.0 in and around Japan (blue circle) from 2008 to 2016, and the 2011 Tohoku M9.0 earthquake (red star).

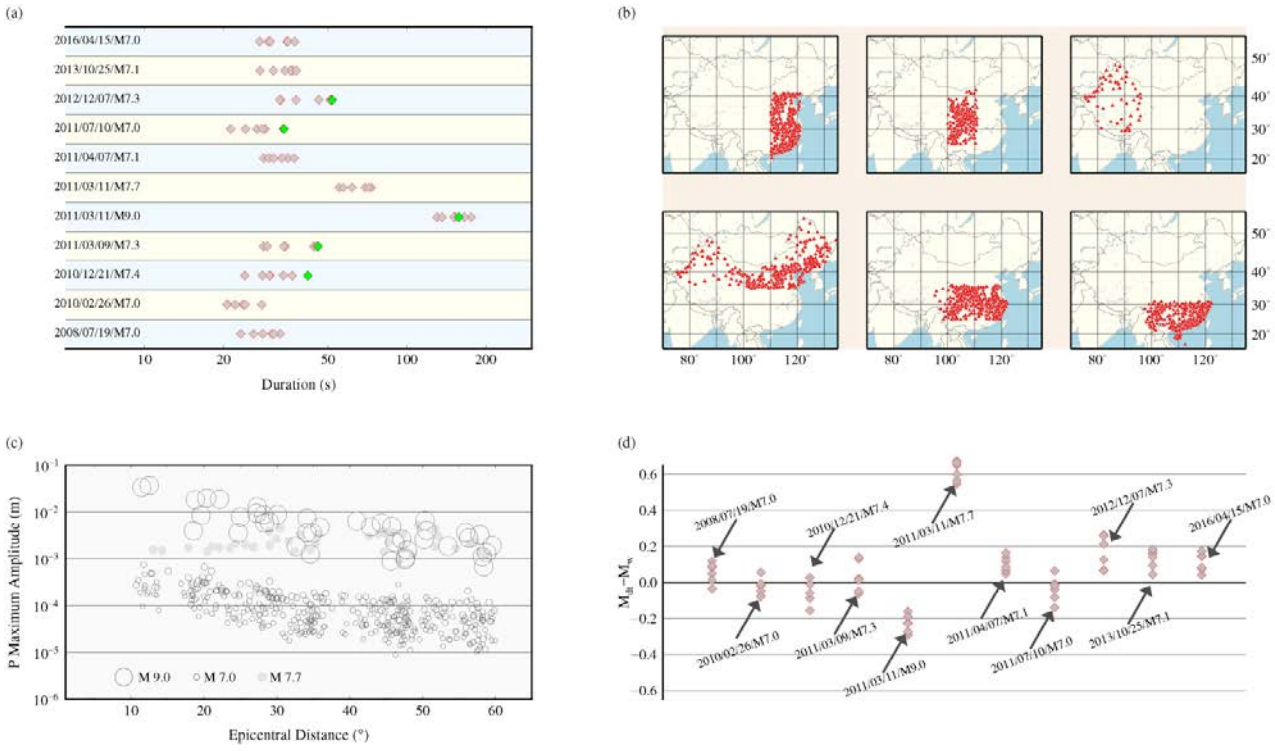

Figure 3.2(a) Source duration derived from back-projection of data recorded at stations showed in (b), green diamonds represent energy duration [*Convers and Newman*, 2013]. (c) the values of the P wave maximum amplitudes. (d) results of comparing M_{dt} with M_w.

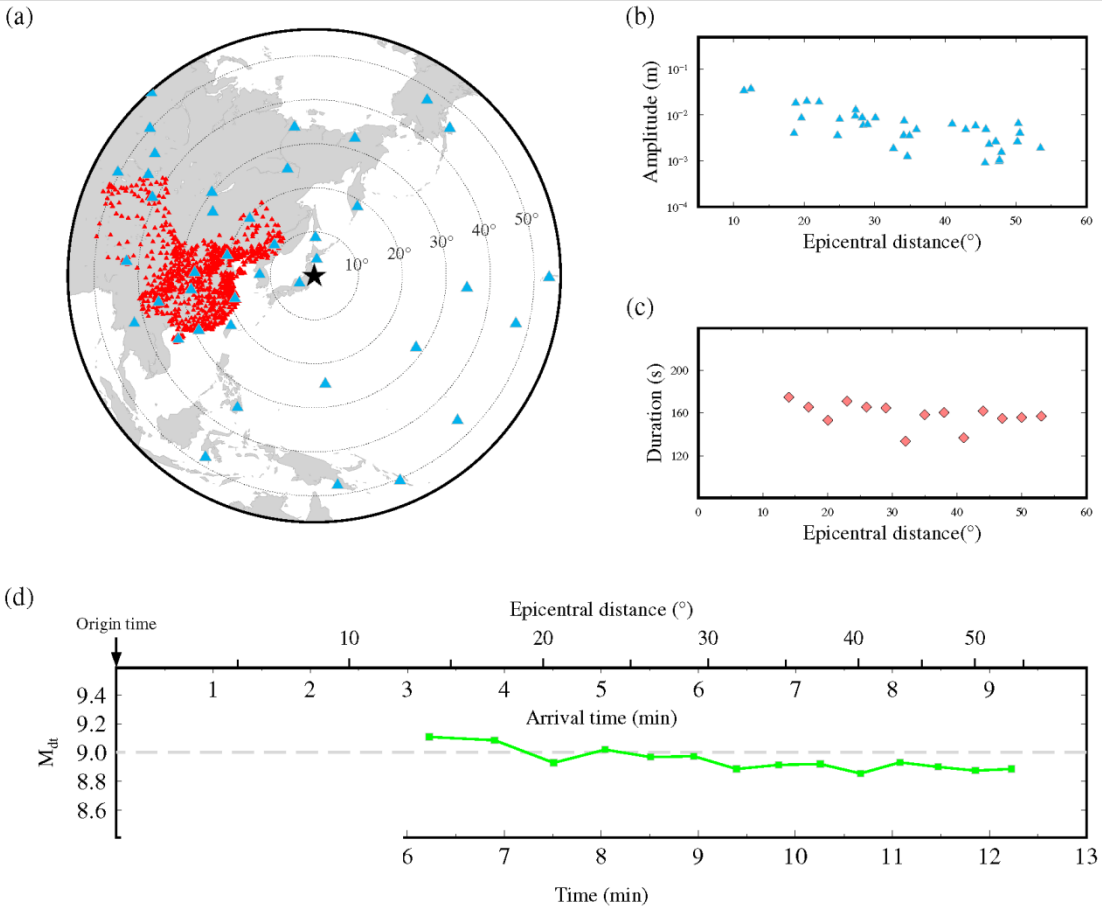

Figure 3.3 Real-time magnitude determining for the 2011 M9.0 Tohoku earthquake. (a) Locations of Chinese (red triangle) and GSN stations (blue triangle). Black lines indicate epicentral distance. (b) Maximum displacement versus elapsed time plot for all P-wave recorded at GSN stations. (c) Time evolution of source duration. (d) Time evolution of M_{dt}.

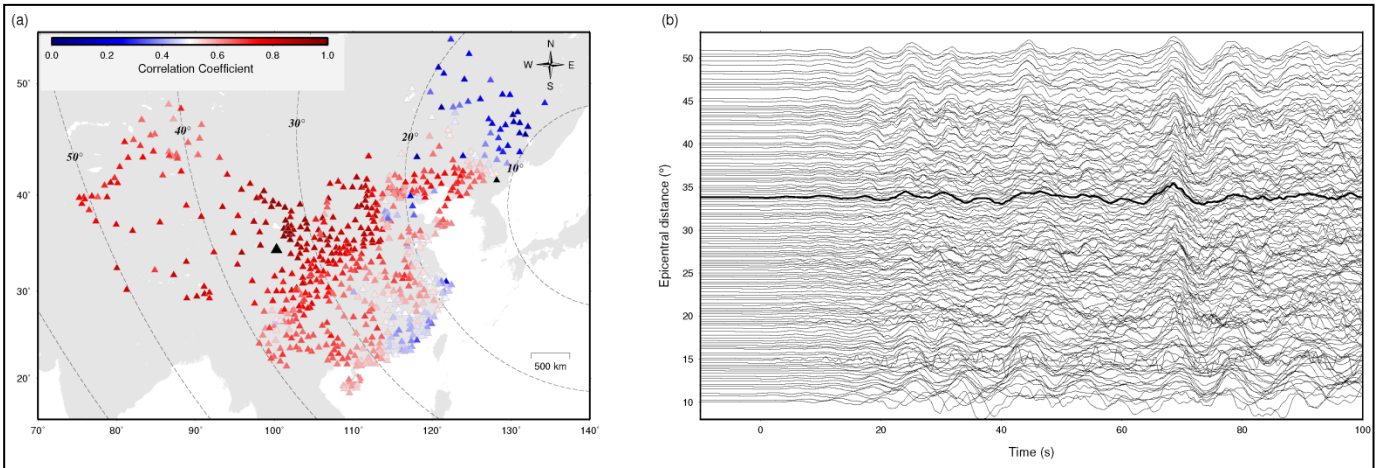

Figure 3.4 (a) Correlation coefficients between waveforms of the 2011 M9.0 Tohoku earthquake recorded at the model station (black triangle) and other Chinese stations. (b) Selected waveforms of the 2011 M9.0 Tohoku earthquake recorded in Chinese stations. Thick black shows waveforms of model station.

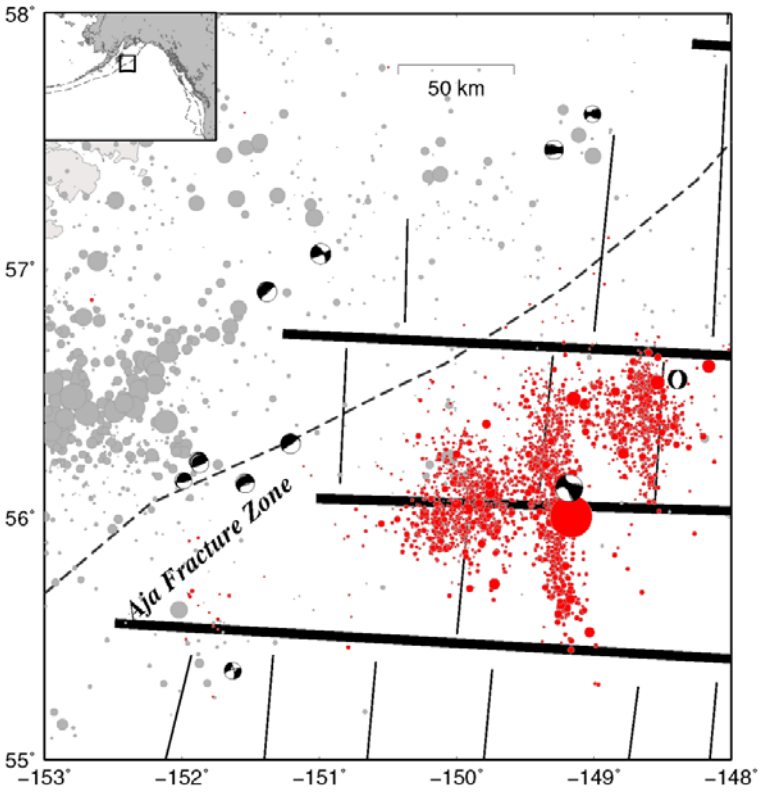

Figure 4.1 Locations of aftershocks (red circles) that occurred within 2.5 months following the main shock and previous seismicity (gray circles) according to the USGS. Bold and thin straight black lines indicate fracture zones, and magnetic lineations, respectively [*Iii and Hayes*, 1968; *Naugler and Wageman*, 1973]. Focal mechanisms are determined by the GCMT.

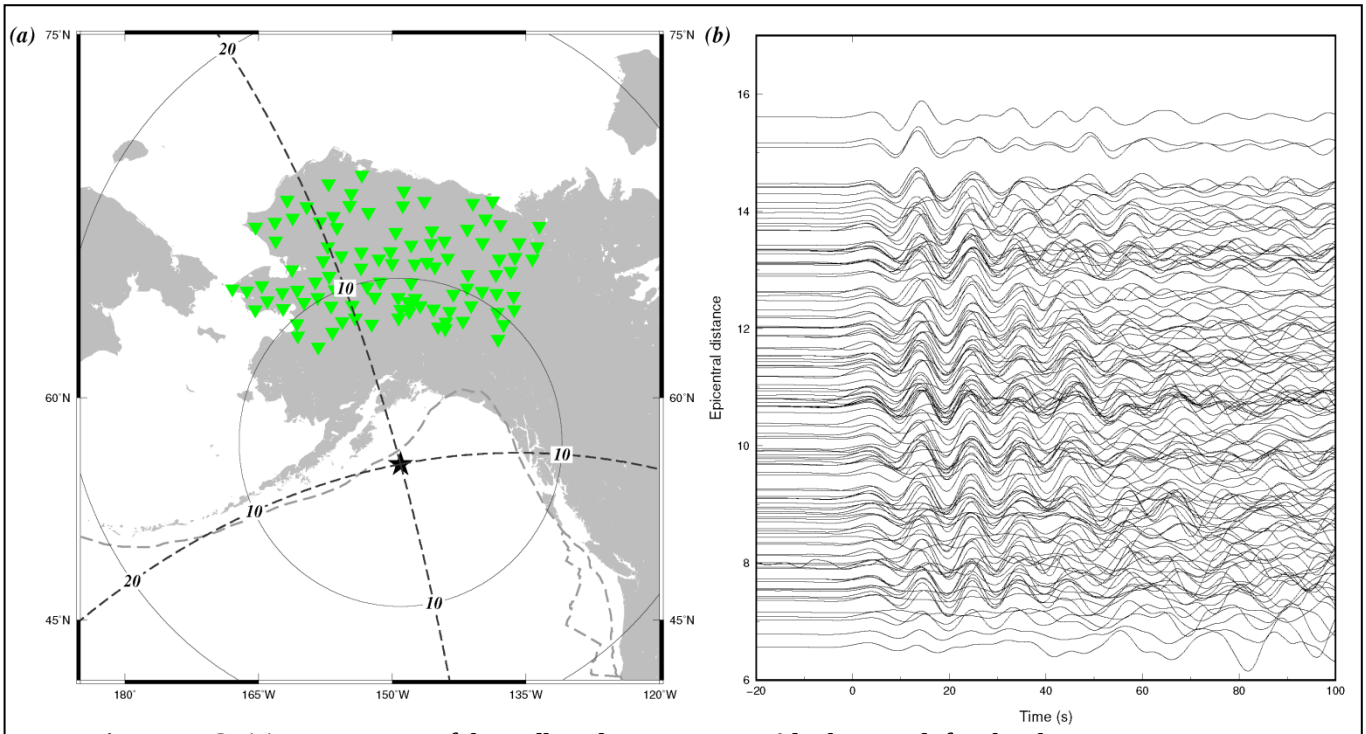

Figure 4.2 (a) Locations of broadband stations in Alaska used for back-projection (green inverted triangle). Solid and dashed lines show the epicentral distances and strikes of the fault planes determined by the GCMT. Large black star shows the epicenter determined by the USGS. (b) Waveforms recorded at stations shown in (a).

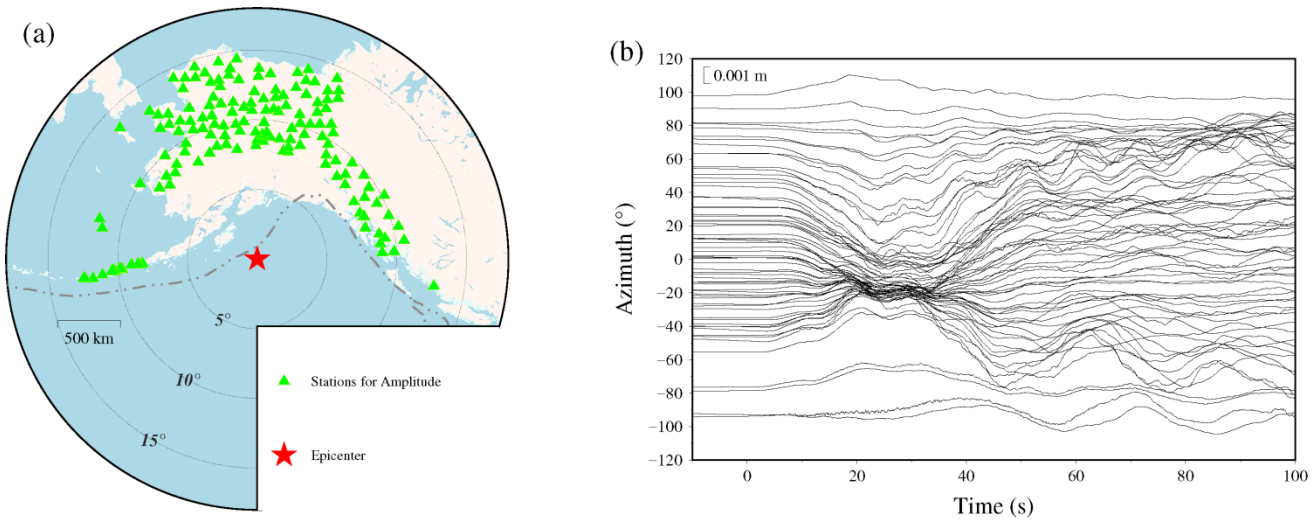

Figure 4.3 (a) Locations of global stations used for calculating the maximum displacement of the P waves. The red star indicates the epicenter for the 2018 M7.9 Alaska earthquake according to the USGS. (b) Displacement waveforms of the P waves recorded at the seismic stations shown in (a).

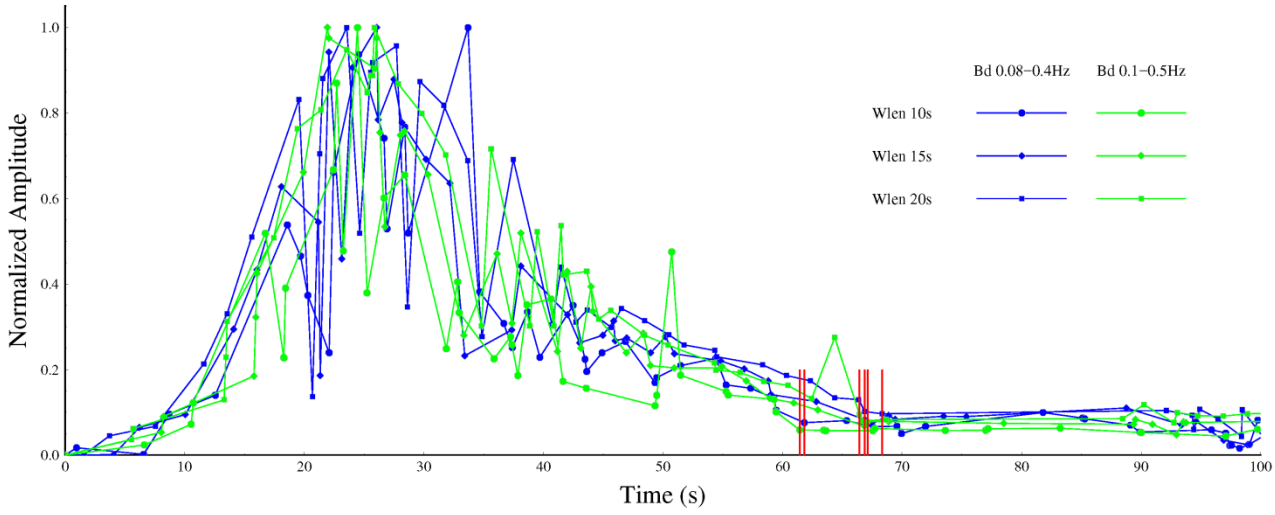

Figure 4.4 Energy-time plots derived from back-projections using stacking length of 10, 15, and 20 s at frequency bands 0.08-0.4 and 0.1-0.5 Hz, respectively. The red lines represent the determined ends of the source according to *Wang et al.* [2017].

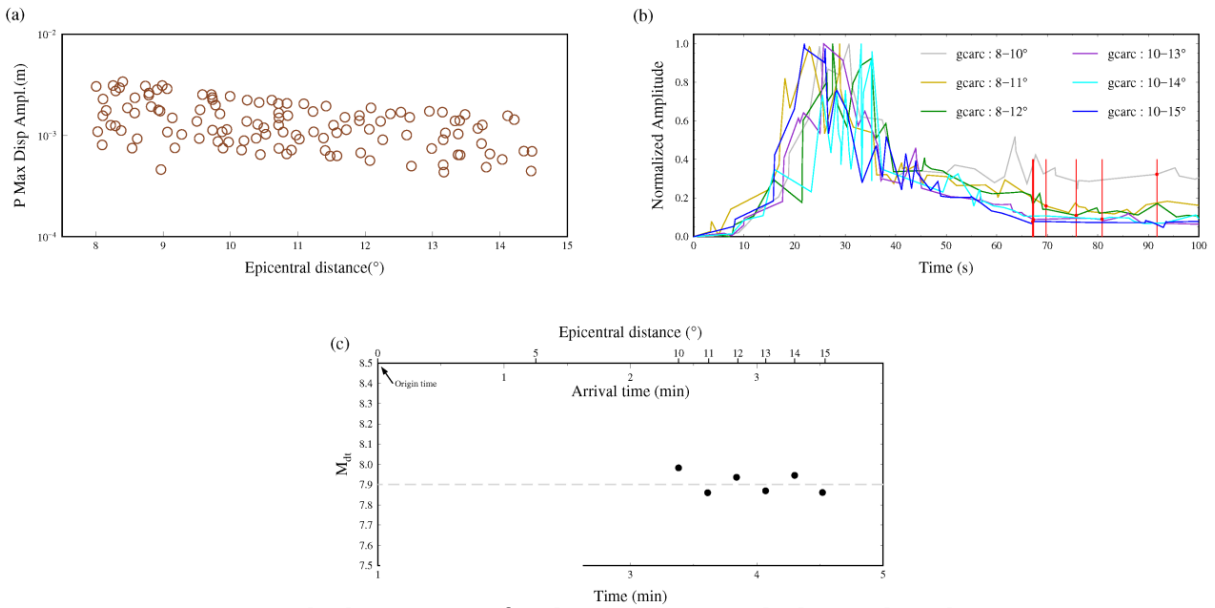

Figure 4.5 Magnitude determining for the 2018 M7.9 Alaska earthquake. (a) Maximum vertical displacement versus elapsed time plot for all P-wave recorded at stations shown in Figure 4.3(a). (b) Energy-time plots derived from back-projections using waveforms recorded at 8-10^o, 8-11^o, 8-12^o, 10-13^o, 10-14^o, and 10-15^o, and filtered at 0.1-0.5 Hz. (c) Time evolution of M_{dt}. The determined magnitude varies from 7.88 to 7.91, consistent with the well-recognized magnitude M_w 7.9. The preliminary magnitude determined by the NOAA is 8.0, which was soon updated as M8.2, and M 7.9 in a few hours.

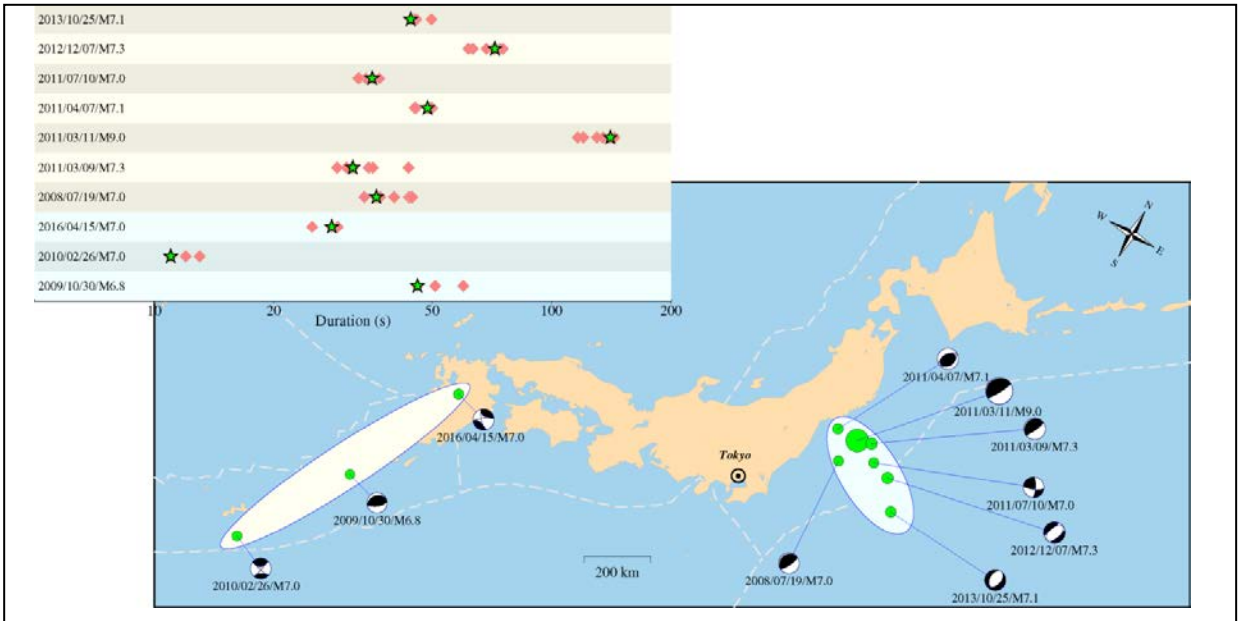

Figure 5.1 Back-projections using station corrections derived from themselves and other nearby earthquakes. Notice that the stations with epicentral distance larger or equal to 30 degrees are used in the back-projections. The 30 October 2009 M6.8 earthquake is added to test. Here pink diamonds and green stars indicate source durations derived from back-projection using station corrections estimated from other earthquakes and themselves, respectively.

1. Introduction

1.1 Global seismicity and seismic stations

Every day there are about fifty earthquakes worldwide that are strong enough to be felt locally, and every few days an earthquake occurs that is capable of damaging structures. An earthquake of magnitude 7 occurs approximately monthly, and an earthquake of magnitude 6 or greater occurs on average every three days [*Pavlis*, 2003].

Earthquakes mostly occur at the boundaries where the tectonic plates converge, diverge, or slide past each other. Although the plates move steadily, their boundaries are often "locked" and do not move most of the time. However, on time scales of a few hundred years, the boundary slips suddenly, and the accumulated motion is released in an earthquake [*Pavlis*, 2003]. **Figure 1.1** shows distribution of the earthquakes (magnitude 6 or greater, from 1990 to 2018) downloaded from USGS earthquake catalog, which roughly define the plate boundaries.

The large shallow earthquakes along the boundaries always are one of most damaging natural disasters all over the world. A recent example is the magnitude 9.0 Tohoku earthquake on 11 March 2011, occurred off the coast of northeast Japan. The earthquake produced a tsunami that struck Japan as well as various locations around the Pacific Ocean, and the tsunami caused massive damage to the nuclear reactors of Fukushima Nuclear Power Plant, which caused releasing of harmful radiation elements and substances into the environment in Japan and all over the world [*Zare and Ghaychi Afrouz*, 2012]. As of July 27, 2011, according to official announcement, fatalities were 15,641 with an additional 5,007 missing. Another example is the 26 December 2004 Sumatra-Andaman earthquake, the damage caused by the earthquake and subsequent tsunami is enormous. 283,100 people were killed, 14,100 were listed as missing, and 1,126,900 were displaced in 10 countries around the rim of the Indian Ocean. Serious damages and death were even reported along the east coast of Africa, as far as 8000 km away from the epicenter [*Wang and Liu*, 2006].

Meanwhile, people have been building more and more seismic dense stations to deal with earthquakes, such as GSN[1], GEOFON[2] network, Hi-net[3] and China array[1] (**Figure 1.2**).

1 GSN: Global Seismographic Network (https://earthquake.usgs.gov/monitoring/gsn/)

3 GEOFON: Global seismological broad-band network operated by the German GeoForschungsZentrum (GFZ) (https://geofon.gfz-potsdam.de/)

3 Hi-net: High Sensitivity Seismograph Network in Japan (http://www.hinet.bosai.go.jp/)

For earthquake early indication, tsunami warning, and other emergency operation, the technology has been making a big progress in rapidly obtaining essential parameters of large earthquakes, like magnitude, focal mechanism, source length and duration [*Duputel et al.*, 2012; *Wang et al.*, 2017; *Wang and Mori*, 2016].

1.2 Magnitude

Among many earthquake parameters, magnitude is a good parameter that represents energy released at the source of the earthquake. From magnitude, people can roughly evaluate fault length, earthquake damage, social response etc.

1.2.1 Problems

Although the method of measuring earthquake magnitude has been applied in 1930s, it still has a large room to develop for rapidly determining magnitude of large earthquakes, which had been fully manifested in follow examples:

At 7:58 on December 26, 2004 (West Indonesia Time), the M9.2 earthquake occurred in Sumatra Island, Indonesia. At 8:15 (about 15 minutes after earthquake), NEIC [2] determined short-period body wave magnitude m_b as 6.1, at the same time, the Indonesia meteorology and disaster management agencies gave the m_b 6.8. At 8:24, NEIC revised the short-period m_b to 6.3. At 9:15 (more than one hour after event), NEIC measured the surface wave magnitude M_s as 8.5. Serious damages and death resulting from the earthquake were mainly attributed to the lack of tsunami warning system in Indonesia.

There was a good tsunami early warning system in Tohoku, Japan, but the tsunami caused by the 2011 M9 earthquake (at 14:46 on March 11, 2011, JST) still destroyed many cities along eastern coast area of Japan. JMA released M7.2 earthquake warning in 31 seconds after earthquake. 140 seconds after the origin time. JMA revised the magnitude to 8.1 and released the last earthquake warning. After 5 hours, JMA adjusted the magnitude up to 8.8 according to analysis of CMT[3]. At 14:49, JMA released the tsunami warning based on the magnitude of 7.9, and then at 15:14, 15:30, 16:08, 18:47, 21:35, 22:53 and 3:20 on next day, the tsunami warning information was upgraded and expanded for times (http://www.jma.go.jp/jma/indexe.html/).

The varied results of magnitude of 2011 Tohoku M9.0 earthquake showed magnitude had been severely underestimated, even in half an hour after event, the value still was 8.1.

1 China array: operated by China Earthquake Administration(CEA) (http://www.cea.gov.cn/)

2 NEIC: National Earthquake Information Center (https://earthquake.usgs.gov/contactus/golden/neic.php/)

3 CMT: Global Centroid-Moment-Tensor (http://www.globalcmt.org/)

Based on this, the tsunami was forecasted about 3-6 meters in height along the coast (Iwate, Miyagi, Fukushima, etc.) closing to earthquake locations by JMA. It is clear now that the largely underestimated tsunami caused the heavy casualties, and the fundamental reason was that the magnitude wasn't determined rapidly and accurately. For subduction zones earthquakes, the main tsunami energy usually reaches the coast in 20-30 minutes after earthquake. Therefore, it is crucial for tsunami warning to determine magnitude rapidly and accurately in ~10 min. If JMA had known more precise magnitude in 10 minutes after earthquake, and then released accurate tsunami warning information immediately, it is highly possible that we could avoid major injuries and loss of engineering facilities during this nature disaster.

1.2.2 Recent methods

Nowadays, with seismic waveforms, the determined magnitude scales mainly include M_L, m_b, M_s and M_w. M_L (local Magnitude) is the earliest magnitude scale, introduced by Charles Richter in 1935 for southern California earthquakes and often referred to as the "Richter scale". For global magnitude scales studies, the primary two were the body wave magnitude, m_b, and surface wave magnitude, M_s. m_b is determined by using the early part of the body wave train, and the surface wave magnitude, M_s, is measured from the largest amplitude (zero to peak) of the surface waves. In general, larger earthquakes radiate a higher proportion of energy at longer periods (lower frequencies) than their smaller counterparts. However, local, body and surface wave magnitudes do not necessarily reflect the real size of large earthquakes because they are derived from short-period (20seconds) amplitudes, saturates beyond a certain limit [*Tsuboi et al.*, 1995]. Moreover, M_L, m_b, and M_s for crustal earthquakes saturate for the same physical reason: for large earthquakes, all of these narrow-band amplitude measurements cannot represent gross faulting characteristic [*Hanks and Kanamori*, 1979].

The moment magnitude, M_w, defines a magnitude scale based on the seismic moment. Seismic moment is a product of the distance a fault moved and the force required to move it. It is derived from modeling recordings of the earthquake at multiple stations. The moment magnitude scale includes the area of the fault's rupture and the slippage along the fault to determine the size of the earthquake's moment. M_w is directly tied to earthquake source processes and does not saturate [*Pavlis*, 2003]. Therefore, M_w has become the common measure of magnitude of large earthquakes. With time, a new moment magnitude, M_{ww}, based on W-phase inversion was established and has been wildly applied in magnitude determining work of large earthquakes in many agencies like USGS, GFZ (GEOFON), PTWC[1], ERI[1] and so on. Generally, it can offer a robust

1PTWC: Pacific Tsunami Warning Center (http://ptwc.weather.gov/)

solution to earthquake magnitude in 20-30 minutes. But at present there are two questions that W-phase inversion method needs to improve. Firstly, the inversion method deals with waveform data using a fixed window length, which causes the errors for earthquakes with long durations. Secondly, since involving low-frequency inversion, the method requires seismic stations to have a wide azimuth range.

In recent years, methods using seismic array has been widely developed, especially in the research on source process and aftershocks detection of large earthquakes. Hara (2007) developed a method to determine earthquake magnitudes using durations of high frequency energy radiation, and maximum displacement amplitudes measured from first arriving P-waves recorded at a tele-seismic distance range. He showed that this method was applicable to huge earthquakes such as the December 26, 2004, Sumatra earthquake (Mw 9.0 after the Global Centroid Moment Tensor Project) [*Hara*, 2007; 2011].

Derived from the method of Hara [2007], *Wang et al.* [2017] proposed a robust algorithm to resolve magnitude, M_{dt} and source length of large earthquakes using seismic data recorded by Hi-net dense arrays and global stations. They tested 74 shallow earthquakes that occurred within epicentral distances of 30–85° to Hi-net (2004–2014). The estimated magnitudes are similar to moment magnitudes estimated from W-phase inversions with standard deviations of 0.14–0.19 depending on the global station distributions. As the results could be produced within 6–13 min (plus the source duration time), the system could be useful for rapid tsunami estimation, shaking damage prediction, and possible practical implementation of emergency response strategies.

1.3 Essay structure

Chapter 1 introduces earthquake hazard and its wide implication across the globe and current methods for determining magnitude. There are many magnitude scales (M_L, m_b, M_s, M_w, M_{dt}), but also many problems in the work of determining large earthquake magnitudes, like magnitude saturation (M_L, m_b, M_s), underestimating magnitude, and low time efficiency in determining magnitude. How to determine magnitude of large earthquake rapidly and accurately? That is the topic that this essay wants to address and discuss.

Chapter 2 introduces the methodology used in the essay. The method can be divided into three parts: first using back-projection to calculate source duration, secondly P wave maximum amplitude, and finally combine them to determine magnitude, M_{dt}.

1ERI: Earthquake Research Institute, University of Tokyo (http://www.eri.u-tokyo.ac.jp/en/)

Chapter 3 and 4 show two cases to analyze the method in details. Former includes 11 large shallow earthquakes occurred in and around Japan, and the seismic data come from Chinese stations and global stations. Later shows that using local and region stations data, I determinate magnitude of Alaska earthquake occurred in 23 January, 2018.

Chapter 5 and 6 introduce the discussions and conclusions of all the work, and suggest that the first release of the tsunami hazard can be evaluated by the more accurate determined magnitude and source parameters such as W-phase inversion based on local observations and our new approach.

Chapter 7 introduces acknowledgements in the thesis.

2. Methodology

As mentioned before, Hara [2007] developed a method to determine earthquake magnitudes using durations and maximum displacement amplitudes. In Hara [2007], source duration was approximated empirically from the envelope of high-frequency waveforms recorded at tele-seismic distances. A good azimuthal coverage and short scattered coda waves that are generated around stations are generally desired for correct estimation of source duration. However, the back-projection can provide accurate estimates of the spatial source length and the source duration in time. Following *Wang et al.* [2017], combining this source duration with the global P wave maximum amplitudes gives better estimate of earthquake magnitudes in terms of time efficiency and robustness.

2.1 Back-projection

Back-projection has been proven efficient at resolving rupture durations and source extents of large seismic sources [*Fan and Shearer*, 2015; *Ishii et al.*, 2005; *Wang et al.*, 2016a; *Wang and Mori*, 2016; *Wang et al.*, 2016b; *Yao et al.*, 2013].

2.1.1 Theory

Here, back-projection method is a simplification of wave field reverse-time migration, aiming to study the time-spatial distribution of energy radiation using waveforms recorded on large regional arrays. Seismograms are stacked for each possible source location to obtain a direct image of the source. Then sum the energy that is radiated from the given source constructively, and cancels out other energy present in the seismograms. That means the back-projection method uses waveforms (usually the direct P arrival) from array data to determine the location of a source that is most consistent with relative timing of the arrival of the seismic waves. It doesn’t require any prior information of fault dimension, fault geometry, or rupture duration [*Ishii et al.*, 2005; *Wang et al.*, 2016a].

The method performs the beam-forming over a sliding or moving window offset to image the stacked energy corresponding to each grid point. Since the obtained time is the local beam time, a time correction to account for the directivity effect in time is necessary because of the varying locations of the seismic sources.

2.1.2 Procedures

The back-projection method assumes that the initial P wave arrival comes from hypocenter, but later parts of the P wave train likely contain overlapping contributions from different parts of the ensuring rupture. In the essay, the back-projection procedure mainly consists of the following steps [*Wang et al.*, 2016a]:

1. Set up points. Make sure the grids surround the whole source area and each grid would be possible source point. Usually, we use the initial epicenter from the USGS.

2. Capture P waveforms recorded at the vertical component, from the whole waveform to avoid interference of later waves.

3. Filter and resample. Mostly we filter high frequency waveform for getting better stacking amplitude.

4. Calculate theoretical travel times from each grid to stations using the 1-D global velocity model IASPEI 1991[*Kennett and Engdahl*, 1991].

5. Compute station corrections and align waveforms. The station correction helps in compensating for structure heterogeneities beneath the stations that affect travel times.

6. Calculate cross-correlation between each station and model station using a window length. Usually we discard stations that have correlation coefficients less than 0.6.

7. Stack the waveforms for a window length. For the stack amplitude, we use the square of the summed amplitudes.

8. Shift the time window and calculate the stack amplitude.

9. Apply a time correction for the directivity effect caused by the progressive change in source position.

For the alignment, the research first crosses correlate waveforms in a relatively lower frequency band, and apply these obtained station corrections to the waveforms. Then, the research crosses correlate for higher frequency bands. This two-step procedure gives a good high-frequency station correction and avoids errors that may be caused by cycle slip in the higher frequencies.

2.1.3 Source duration

The back-projection results can accurately estimate the rupture process (rupture length, rupture velocity), energy-time plot. The research determines the source duration based on the energy-time plot (proxy of source time function) derived from the back-projection. The research calculated source duration, in which 90% of the total energy has been included, and another duration, in which the amplitude of the total is smaller than 0.1 time of the maximum stacked energy and 80% of the total energy has been included. The research defines the shorter one as the source duration.

There are two advantages for back-projection to calculate source duration. First, the source duration can be determined accurately by seismic arrays. The duration of envelopes of high-frequency waves are affected frequently by possibly strong site effects and directivity effects at global stations. Therefore, many stations at different azimuthal locations were required to acquire good estimates of earthquake magnitudes in Hara [2007]. The back-projection method inherently accounts for directivity effects and minimizes the coda waves generated at individual array stations. Second, the results can be calculated more rapidly.

2.2 Global distributions of P wave amplitudes

Global stations are generally distributed in all azimuths of earthquakes. After removing the instrument responses, the research obtains the maximum displacement from the predicted arrivals of P to S waves using the software Taup [*Crotwell et al.*, 1999] and 1D velocity structure model IASPEI 91[*Kennett and Engdahl*, 1991] (**Figure 2.1**).

2.3 Estimating magnitude

This research determinate the magnitude by combining the maximum amplitude of the P waveforms and source durations derived from back-projection. Here I follow an equation (**Figure 2.2**) of *Wang et al.* [2017], and detailed equations as below:

$$K^1 = \frac{0.53}{N_1}\sum_{i=1}^{N_1} log\, A_i \; + \frac{0.44}{N_1}\sum_{i=1}^{N_1} log\, \Delta_i + 1.01\, log(duration) + \; 6.23, \qquad (1)$$

$$K^2 = \frac{0.51}{N_2}\sum_{i=1}^{N_2} log\, A_i \; - \frac{0.01}{N_2}\sum_{i=1}^{N_2} log\, \Delta_i + 1.05\, log(duration) + \; 7.89, \qquad (2)$$

$$M_{dt} = \frac{K^1 + K^2}{N_1 + N_2}, \qquad (3)$$

Where A_i is the maximum vertical displacement of P wave recorded at the i_{th} station, and Δ_i is the epicentral distance (km). N_1 and N_2 are numbers of the stations with epicentral distances of up to 40^o, and 40^o to 85^o, respectively. The operator log denotes the decimal logarithm.

3. Real-Time Estimation of Magnitudes of Large Earthquakes in and around Japan Using Dense Chinese Seismic Stations

3.1 Background

3.1.1 Seismicity in Japan

Japan is an earthquake prone country, with 20~30 M>=7 and 200~300 M 6-7 earthquakes in the past 20 years, among which, the 11 March 2011 M9.0 Tohoku earthquake caused several damages along the coast of the north Japan. The M9.0 Tohoku earthquake occurred off the coast of northeast Japan, caused around 30, 000 deaths and over trillion dollars in damage, making it one of the most damaging earthquakes ever recorded. The tsunami first reached the Japanese mainland 20 min after the earthquake and ultimately affected a 2000 km stretch of Japan's Pacific coast [*Mori et al.*, 2011]. Coast areas at latitude 38 to 40 degrees were experienced tsunami with run up height at least 20 m, where Miyako area showed the maximum run-up height of 39.7 m. Many coastal tide gauges on the Pacific coast stopped recording after the first tsunami with > 9 m amplitude, because of power failure or because the stations were washed away by the tsunami [*Fujii et al.*, 2011].

3.1.2 Magnitude problem

As represented in chapter 1, the large damages in tsunami were partly due to the tsunami height estimation based on M7.9 led to delay of evacuation (The 2nd Export Group Meeting on the Great East Japan Earthquake, 16-18 December 2011). There was a large underestimation for the magnitude of the 2011 M9.0 Tohoku earthquake in the initial stage. 3 min after the origin time, the Japan Metrological Agency (JMA) identified this earthquake with a magnitude of 7.9 (The 2nd Export Group Meeting on the Great East Japan Earthquake, 16-18 December 2011). 4.7 min after the origin time of the 2011 M 9.0 earthquake, the U.S. Geological Survey National Earthquake Information Center (USGS NEIC) and Pacific Tsunami Warning Center (PTWC) released the first magnitude estimate of M_{wp} 7.5. 18.6 min after the origin time, several magnitude estimates including m_b (L_g), m_b, m_L, m_B and M_{wp} [*Tsuboi et al.*, 1995] were computed by the NEIC and JMA using more data, all below M 7.8 except M_{wp}, which was estimated

as 8.3. 32 min after the origin time, Mw 8.9 was estimated from the centroid moment tensor inversion algorithm at the USGS based on the inversion approach of Jascha Polet, which indicated a mega-earthquake [*Hayes et al.*, 2011].

However, even for the methods that don't need Green's functions and inversion, the earthquake location information is required. For example, in *Wang et al.* [2017], the epicenter location is used to calculate station corrections for the stations in the Hi-net array to account for the structure heterogeneities that is not considered in calculating travel times [*Kennett and Engdahl*, 1991]. Therefore the first estimate of magnitude relies largely on prompt and correct identification of the seismic events, increasing risk on wrong estimation of source sizes.

Here the research tests this procedure to 11 M ≥ 7.0 (USGS) shallow earthquakes that occurred in and around Japan from 2008 to 2016, using seismic data recorded in China and across the globe.

3.2 Data and Method

All of the 11 M ≥ 7.0 shallow earthquakes (USGS) occurred in and around Japan from 2008 to 2016 are analyzed (**Figure 3.1**). Among these earthquakes, there were eight earthquakes distributing offshore of the east coast of Honshu, Japan, including the 2011 Mw 9.0 Tohoku, Japan earthquake.

The research downloaded seismic data recorded by the vertical component of the dense regional broadband seismic stations in China [*Zheng et al.*, 2010] for the 11 earthquakes from the Data backup center of Institute of Geophysics, China Earthquake Administration (IGCEA). There are about 1000 Broadband seismic stations, which are at epicentral distances of about 10 to 60 degree on average. For the March 11, 2011, M9.0 earthquake, The Chinese stations are located at distances of 10 to 51 degree and azimuth range of 238 to 332 degree. The sampling ratio is 100 Hz for all of the stations. The research downloaded broadband vertical components (BHZ) of the direct P wave data from the Global Seismograph Network (GSN) stations, from IRIS DMC (Incorporated Research for Seismology, Data Management Center). For every earthquake analyzed, there are at least 40 GSN stations in the epicentral distance of 10 - 60 degrees. Close broadband stations (say less than 10 degrees) are easy to be off scaled for Giant earthquakes, like the 2011 M9 Tohoku, Japan earthquake. So the research chooses global stations with epicentral distances large or equal to 10 degrees, to avoid the risk of off scale problem.

The research basically follows *Hara* [2007b], estimating earthquake magnitude using source duration and maximum displacement of P waves. The difference is that The research estimates the source duration by performing back-projection in large regional array [*Wang et al.*, 2017]. By stacking a large number of waveforms, back-projection method can overcome potentially strong site effects, cancel out coda waves, and consider the directivity effects in waveforms, therefore obtains source duration in high resolution [*Fan and Shearer*, 2015; *Honda et al.*, 2011; *Ishii et al.*, 2005; *Koper et al.*, 2012; *Krüger and Ohrnberger*, 2005; *Meng et al.*, 2011; *Satriano et al.*, 2012; *Yagi and Okuwaki*, 2015; *Yao et al.*, 2013; *Zhang et al.*, 2011]. Another advantage in the new method is that it doesn't require many global stations, as tested in [*Wang et al.*, 2017].

The procedure consists of the following steps:

1. Back-project seismic data recorded at the vertical component of the stations in China to get the source durations. The frequency band applied to the waveforms for stacking, length of stacking window, and the sampling interval, are 0.5-2.0 Hz, 10 s, and 0.01 s, respectively. I set a coefficient threshold of 0.4 to eliminate noisy data. I set a horizontal grid net at hypo depth. From the onset of the P wave, I performed back-projection using 10 s time windows that are offset by 1 s. The total length of the window for stacking is two times of the predicted source duration following *Wells and Coppersmith* [1994]. The travel times between grid points and stations are calculated using the 1D velocity structure model IASPEI 91 [*Kennett and Engdahl*, 1991].The source duration is determined from the energy-time plot (proxy of source time function) derived from the back-projection.

2. Calculate the maximum displacements of the direct P-wave recorded across the globe. After removing the instrument responses, the research obtained the maximum displacement from the predicted arrivals of P to S waves that are estimated from 1D velocity structure model IASPEI 91 [*Kennett and Engdahl*, 1991].

3. The research combined earthquake source duration with the P-wave maximum displacements to compute M_{dt} via

$$M_{dt} = \frac{0.55}{N}\sum_{i=1}^{N_1}\log A_i + \frac{0.67}{N}\sum_{i=1}^{N_1}\log \Delta_i + 1.01\log(T) + 5 \quad (1)$$

Here A_i is the maximum amplitude of the P wave at the i_{th} station, with distance of Δ_i; N is the number of global stations involved in the estimation.

3.3 Magnitudes for large earthquakes in Japan from 2008 to 2016

To better estimate the uncertainties of the source durations derived from back-projection, I divided Chinese stations into 6 groups based on station distribution to evaluate the effects of station distributions on the source durations (**Figure 3.2**). The obtained source durations are generally similar to the ones determined by the energy durations by *Convers and Newman* [2013]. For M 7.0-7.4 earthquakes, the values of the P wave maximum amplitudes in the epicentral distance of 10-40 degree are between 10^{-5} and 10^{-3} m, and mainly from 10^{-5} to 10^{-4} m in the epicentral distance greater than 40 degree. For M9 earthquake, the amplitudes are in a range from 10^{-3} m to 10^{-1} m in the 10-40 degree and from 10^{-4} m to 10^{-2} m in the epicentral distance greater than 40 degree. But for the 11 March 2011 M7.7 earthquake, occurred in 39 minutes after 2011 Mw 9.0 Tohoku earthquake, its waves were affected by latter's coda, resulting in displacement became larger and all amplitudes fluctuated near 10^{-3} m.

Considering the source variations, the uncertainties in the determined magnitudes are ~0.2 except for the 11 March 2011 M7.7 earthquake (Figure3.2 (d)). Because the waveforms are overlapped by the surface waves of the 2011 M9 Tohoku earthquake, the source duration and the maximum displacement of the P wave are significantly elongated/enlarged, resulting in a much large M_{dt}.

3.4 Magnitude variation with elapse time for 2011 Mw 9.0 Tohoku earthquake

The research generated a real time environment to mimic the variation of the determined magnitude of the 2011 M9.0 Tohoku earthquake using the Chinese stations and GSN stations (**Figure 3.3**). The closest station is ~ 10^{o} from the epicenter, where the P waveform arrived at 145 s after the origin time. I start to perform the back-projection 3 min after the origin time, among which eight regional stations are used. The source duration is determined as 175 s. There are only two GSN stations available in the distance. Maximum displacements recorded at the two GSN stations are in the range of 0.01~0.1 m. From them I estimate a magnitude of 9.1, which agrees well with Mw 9.0 issued by JMA and from the USGS W-phase moment solution, and 9.1 from the Global CMT.

Then I performed back-projection when the P wave reaches 3 more degrees (~ half a minute), to update the back-projection results, and re-estimate the magnitude using the new source duration and more maximum displacements of the P wave as the seismic waves traveled further and reached more GSN stations with time. The estimated source duration is as long as 175s at first and decreased with elapse of time, but eventually stabilized at 165s. The maximum displacements of the P wave are between 0.001 to 0.1 m. The estimate of the magnitude is stabilized at 8.9 6 min after the origin time, very

similar to the M 9.0 determined by the USGS and Global CMT. To be sure, when epicentral distance is greater than 30 degree, the stations within 30 degree were not used gradually because of low correlation coefficients (**Figure 3.4**).

The fluctuation of determined magnitude (8.9-9.1) in our method 6 min to 12 min after the origin time is no larger than those of the standard approaches such as moment magnitude estimated from the centroid moment tensor and W-phase inversions 20 min to 2 days after the origin time [*Hayes et al.*, 2011].

2. Magnitude of the 23 January 2018 M7.9 Alaska earthquake estimated by local dense seismic stations

4.1 Background

The Gulf of Alaska is located in Pacific plate. The Pacific plate subducts beneath the North American plate at longitude west of 146^{o} W along Aleutian trench, giving rise to extremely large megathrust earthquakes and many intermediate earthquakes [*Freymueller et al.*, 2008]. The plate motion of the Pacific plate relative to the North American plate is ~ 5.6 cm/yr in the direction of 350^{o} at the eastern end of the Aleutian trench [*Pegler and Das*, 1996], showing complicated geodynamic environment along the trench.

On 23 January 2018, the Mw 7.9 earthquake occurred in the offshore region of the Kodiak, south Alaska. No foreshocks were recorded according to the earthquake catalogue issued by the United States Geological Survey (USGS). Up to 10 April 2018, there were 14 M5-6, 211 M4-5, and ~2000 M3-5 aftershocks (**Figure 4.1**).

Magnetic survey showed clear magnetic lineations between 152^{o} W and 142^{o} W, indicating a series of East-West trending fracture zones including the Aja fracture zone and three other linear fractures with similar orientation [*Iii and Hayes*, 1968; *Naugler and Wageman*, 1973]. Magnetic anomalies along both sides of the fractures suggest right-lateral strike-slip offsets on the order of a few tens of kilometers to ~ 200 km. The earthquake sequence seems ruptured several conjugate faults including the East-West trending fractures and the ones parallel to the magnetic lineations, as indicated by the complex locations of aftershocks. The focal mechanism derived from Global CMT shows a strike-slip faulting, agreeing well with the fracture behavior in the source region.

At 12:31:43 am, 23 January 2018, the earthquake rupture began. At 12:35 am, National Oceanic and Atmospheric Administration (NOAA) issued the first tsunami warning for BC, southeast Alaska, and Aleutians based on M=8 and offshore location. At 13:05 pm, NOAA issued the second tsunami warning based on M=8.2 and offshore location. At 14:18, largest tsunami wave observed in Sitka at 0.4 ft height. At 14:19 pm, NOAA issued the third tsunami message based on M=7.9 and offshore location.

In this work, I apply above approach to determine the magnitude for the earthquake, using stations recorded at local to regional dense seismic stations. Dense seismic stations in Alaska help better estimate of the source duration since the coda waves are cancelled out in the procedure of stack during the back-projection.

The first estimate of the magnitude is 8.03 in 3-4 min after the origin time. 4 min after the origin time, the magnitude is estimated as 7.87. The final estimate of the magnitude is 7.86 using all stations in and around Alaska at epicentral distances up to 15 degrees. Our method shows quite stable and rapid estimate of the magnitude for the earthquake, indicating a promising aid for source parameterization in tsunami warning and hazard assessment.

4.2 Data and Method

4.2.1 Data

I use seismic data recorded in and around the Gulf of Alaska, US. There are ~ 258 broadband stations in the Gulf of Alaska, western Canada, and along the Aleutian trench. Stations with azimuths of -40^o to 35^o and epicentral distances of 8^o to 15^o are used for back-projection (**Figure 4.2**). All of the stations at distances of 8^o to 15^o are used to calculate the maximum displacements of the direct P waves (**Figure 4.3**).In this study, we want to investigate how well the local to regional stations work for determining magnitude in the new approach, therefore the farther stations that are available in the Incorporated Research Institutions for Seismology (IRIS) are not used.

4.2.2 Method

Following *Wang et al.* [2017], I first determine the source duration by back-projecting the seismic data recorded in the Gulf of Alaska. The hypocenter (-149.166^o, 56.004^o, 14.1km) determined by the U.S. Geological Survey (USGS) is used in this work. We first set up a horizontal grid of 20*20 points cover the possible source area at depth of 14.1 km. The interval between grids is 15 km. The back-projection method doesn't have good resolution in depth, so the assumed horizontal grid doesn't significantly affect the resolution in horizontal plane and of the source duration. I use the software TauP [*Crotwell et al.,* 1999] and the velocity structure IASPEI 1991[*Kennett and Engdahl*, 1991] to calculate the travel time between grid points and the seismic stations. In order to overcome the structure heterogeneities beneath the Alaska stations that are not taken into account in the IASPEI 1991 velocity model, we apply a station correction procedure [*Fan and Shearer,* 2015; *Ishii et al.,* 2005; *Satriano et al.,* 2012; *Wang et al.,* 2016a; *Yao et al.,*

2013; *Zhang et al.*, 2011] to further improve the travel time calculations. I align the first 60 s and 10 s after P arrivals of the waveforms to the epicenter with filters 0.05 to 0.5 Hz, and 0.1 to 0.5 Hz, respectively, to constrain the initial source location to the epicenter determined by the USGS. In this step, I eliminate noisy waveforms with correlation coefficients less than 0.6 to the model waveforms (station COLD, Longitude：-150.201°, Latitude 67.2278°) for the other waveforms filtered in the frequency band 0.1 to 0.5 Hz.

To obtain the source migration, I use a time windows that are offset by 2 s. By comparing the stacked energies for the tested grid points, I trace the rupture energy release in space and time, therefore estimate the source duration [*Krüger and Ohrnberger*, 2005]. Following *Wang et al.* [2017], I determine the source duration based on the energy-time plot (proxy of source time function) derived from the back-projection. I calculate source duration, in which 90% of the total energy has been included, and another duration, in which the amplitude of the total is smaller than 0.1 time of the maximum stacked energy and 80% of the total energy has been included. The research defines the shorter one as the source duration.

For the seismic data recorded at distance of 8^o to15^o and azimuth of -97^o to 98^o, I remove the instrument responses, and calculate the maximum displacement for the waveforms from theoretically estimated P arrival to S arrival.

4.3 Magnitude estimation

After obtaining the source duration and maximum amplitudes of direct P waves, I use equation (2) in chapter 2 to estimate the M_{dt}. Using the stations distributed in the distance range of 8^o to 15^o and at azimuths of -97^o- 98^o, and the source duration of 67 s estimated for the back-projection results, M_{dt} is estimated as to be 7.86.

I test how the selected frequency bands and length of stacking widows affect the resolution of the back-projections and therefore the uncertainties in source duration, I choose another frequency band of 0.08 – 0.4 Hz, and window length of 10, 15, and 20s, and perform back-projection to evaluate the variations for the determined source durations (**Figure 4.4**). The source durations show little variations between 62 and 68 s, around 0.95 -1.05 times of the source duration (65 s) estimated from the entire stations, which affect the M_{dt} varying -0.02 to 0.02.

I mimic a real time environment to estimate the M_{dt} in real time, and evaluate the accuracy of the estimated magnitude over time (**Figure 4.5**). When the direct P wave arrived 33 stations that are 10^o from the epicenter in the Gulf of Alaska (3 min after the origin time), I start to perform back-projection. The estimated duration is 91 s. Together with 68

maximum amplitudes of the direct P wave recorded in global stations, I estimate the M_{dt} 8.03. 4-5 min after the origin time (P wave traveled 11 degrees away), with 73stations in back-projection, and 94 global stations, the M_{dt} is estimated as 7.94. The final estimate of M_{dt}, using the entire stations in and around the Gulf of Alaska in azimuth of -69^{o}- 71^{o} and distance of 10-15 degree, is 7.86. The magnitude fluctuation of 7.86-8.03 is very accurate, and therefore can be used for the purpose of tsunami warning and hazard evaluation.

Here I combine the source duration and maximum displacements of direct P waves to calculate magnitude (M_{dt}). Magnitude can be estimated from the source duration following *Ekström et al.* [1992] and *Hanks and Kanamori* [1979], although the complexities of frictional prosperities in fault planes distort the resolutions sometimes. Given a source duration of 62 - 68 for this earthquake, the estimated magnitude would be 8.25 –8.33, which shows a large variation to the well accepted magnitude (Mw 7.9). Mw, estimated by W-phase inversion in USGS, shows a magnitude of 7.9, which is similar to the value of 7.87 – 7.95 determined from Global CMT method which utilizes the full waveforms. The M_{dt}, Mw from W-phase, and Mw from Global CMT for this earthquake resemble, indicating the effectiveness of this newly developed magnitude scale for rapid determination of large shallow earthquakes.

5. Discussions

5.1 Station correction

In the present methodology such as in *Wang et al.* [2017] and in the above determining process, earthquake location is needed to calculate station corrections. I guess that station corrections can be estimated by previous moderate earthquakes that occurred in the interested region. The research chooses the 7 earthquakes that occurred in the source region of the 2011 Tohoku earthquake and 3 earthquakes closing to China, to calculate the station corrections. The research performs back-projection using station corrections derived from the other stations. The source durations derived back-projections using from the station corrections of other earthquakes show similar values as the ones derived from back-projection using their own station corrections (**Figure 5.1**), although there are notable variations for some earthquakes due to local structure heterogeneities [*Fan and Shearer*, 2017]. Those results validate the hypothesis that pre-stored station corrections are good enough for fast estimate of source durations of earthquakes. Given a pre-stored database of station corrections with well distributed moderate earthquakes, the algorithm of determining magnitude can run in an automated fashion without earthquake catalogue information. Developing such an automated real time back-projection system using dense stations in China, will largely improve the accuracy and speedy the time of estimating the size of large to giant earthquakes in earthquake prone area in East Asia such as Japan, offering precise source parameters for tsunami hazard evaluation.

5.2 Method comparison

An advantage of this method other than W-phase and Global CMT is that the magnitude of large earthquakes can be estimated in a straightforward way rather than implementing inversion. Together with the magnitude, the source extent, and distribution of high frequency energy radiation can be estimated at the same time. Magnitude, source extent, and source duration sketch the general features of rupture process. For example, divide the source length by the source duration, one can obtain rupture speed. Knowing the source extent and fault layouts would greatly improve the accuracy of fast slip inversion. There are a few groups working on fast slip inversion that offer fault slip models in a few hours after the origin times of earthquakes (such as the USGS). Based on previous seismicity, focal mechanisms, and known surface faults, they assume the fault plane,

and then invert the slips in the fault plane. Or invert slips on each nodal plane of the focal mechanism, and the one with better waveform fittings is recognized as the fault plane. However, fault complexities exist, which is seldom considered or difficult to be evaluated due to limited resolution in the inversion, especially when local data are not available. Recently, with better observations and back-projection methods, many large earthquakes show complicated patterns with more than one fault. For example, the 11 April 2012 M 8.6 Off Sumatra and the 13 November 2016 M 7.8 New Zealand earthquakes has evolved at less 4 and 13 faults, respectively [*Hamling et al.*, 2017; *Satriano et al.*, 2012; *Wang et al.*, 2018]. For the 23 January 2018 M7.9 Alaska earthquake, the aftershocks also show complex pattern, suggesting a multi-fault rupturing during the earthquake. With array technology, fault pattern (fault planes) can be obtained in details, therefore help the correct configuration of the fault model. Incorporating the fault pattern from the back-projection, can improve the accuracy of fault models in fast slip inversion, and help better estimate the slips in the fault plane(s). This improvement will also refine accurate estimate of Moment magnitude.

6. Conclusions

Large shallow earthquakes are one of most damaging natural disasters. Rapid determination of earthquake magnitude is of importance for estimating shaking damages, and tsunami hazards in coastal countries and regions. Usually those approaches regard the source as point source, and suffered from saturations. The most accurate estimate of size of earthquakes would be moment magnitude (M_w). However, there still are a few problems for accurately estimating magnitude of large earthquakes right after large damaging earthquakes. Wang et al. [2017] proposed a robust algorithm to resolve magnitude, M_{dt} and source length of large earthquakes using seismic data recorded by Hi-net dense arrays and global stations. The system could be useful for rapid tsunami estimation, shaking damage prediction, and possible practical implementation of emergency response strategies.

Based on the methodology of Wang et al. [2017], the essay analyzed two cases to determine magnitudes of large earthquake rapidly and accurately. One is 11 M≥7.0 shallow earthquakes that occurred in and around Japan from 2008 to 2016, using seismic data recorded in China and across the globe. The other is the 23 January 2018 M7.9 Alaska earthquake using seismic stations recorded at local to regional distances in Alaska, US.

For Japanese earthquakes, the results agree well with the M_w estimated from W-phase inversion, with a standard deviation of 0.19, and suggest that the magnitudes can be accurately estimated in 6 to 12 min after origin times of earthquakes, depending on the epicentral distances to seismic stations in China. Using station corrections derived from the other earthquakes that occurred Off-Miyagi area, we observe that the source durations don’t show much variations. The source durations can be resolved by using station corrections estimated from previous moderate earthquakes that occurred nearby.

Therefore the essay proposes to build an automated system for real time back-projection using real time seismic data recorded in Chinese stations, and a pre-stored database of station corrections derived from previous moderate earthquakes. Together with stations in Global Seismological Network (GSN), magnitude of large to mega earthquakes in and around Japan can be automatically estimated in real time.

For the Alaska earthquake, in our method, the first release of the magnitude (M_{dt}= 8.03) can be determined in 3-4 min. The M_{dt} is updated as 7.87 in 5 min after the origin time. For the purpose of tsunami warning, resolving accurate magnitude of earthquakes in 5-10 min might be acceptable for a timely tsunami warning. For example, for the 2006 M 7.7 Java earthquake, the damaging tsunami waves reached the coast areas at ~30 min after the origin time. For the 2011M 9.0 Tohoku, Japan earthquake, large tsunami waves first reached Miyako at 20-30min after the origin time.

Therefore, multiple regional dense arrays around the world are necessary for monitoring global earthquakes. Currently, there are a handful of regional networks that are available for this purpose, such as the dense broadband stations in Europe, China, Australia, and the U.S. With multiple dense stations, response times could be minimized. It has been proved in Chapter 3 that the China Array can determine source information within 10 min for large earthquakes (with source duration of less than 4 min) that occur in and around Japan, while it would take an additional 6 min if U.S. data are used because the greater distance requires more time for the direct P waves to arrive.

Earthquake early warning algorithms probably offer the fastest results for earthquake sizes, however with great uncertainty. The release of incorrect warning information would greatly destroy the confidence of the public on the warning system. Considering that more accurate estimate of magnitude can be obtained in a few minutes after origin time and ~30 min delay for the damaging tsunami waves reaching coast areas, here suggests that the first release of the tsunami hazard is evaluated by the more accurate determined magnitude and source parameters such as W-phase inversion based on local observations and our new approach.

7. Acknowledgements

First of all, I would like to extend my sincere gratitude to my supervisor, Dun Wang, for his patient and generous guiding, including Generic Mapping Tools (GMT), Seismic Analysis Code (SAC), Computer Programming (Fortran language), all academic methods in the essay. I feel grateful to all the teachers in the China University of Geosciences (Wuhan), who offered me valuable courses during my undergraduate studying. Also thank staffs in School of Earth Science for their considerate service.

Secondly, all the work were supported by NSFC grants 41474050 (C.S., D.W), the Fundamental Research Funds for the Central Universities, China University of Geosciences (Wuhan) CUG170602 (Q.Y., D.W.), and National Program on Global Change and Air-Sea Interaction (GASI-GEOGE-02). We thank the Data Management Centre of China National Seismic Network at Institute of Geophysics (SEISDMC, doi:10.11998/SeisDmc/SN), China Earthquake Networks Center, China Earthquake Administration. Global station data were obtained from the Incorporated Research Institutions for Seismology (IRIS). Focal mechanisms are from the Global CMT website (Last accessed at April 2018). Earthquake catalogues are downloaded from the USGS website (Last accessed at April 2018).Comments from the Hitoshi Kawakatsu, Jim Mori, Alex, Hulko, Chengli Liu greatly improved the thesis.

Last but not least, I really enjoyed days with classmates and I gained a lot from them. Likewise, my sincere thanks should go to my beloved friends and parents who have always been greatly supporting and caring for me all my life.

References

陈运泰, 刘瑞丰 (2004), 地震的震级, 地震地磁观测与研究, 25(6), 1-12。

杜海林,许力生 (2012), 日本大地震震源破裂过程的台阵技术成像, 国际地震动态 (6), 21-21。

龙锋, 闻学泽,徐锡伟 (2006), 华北地区地震活断层的震级-破裂长度、破裂面积的经验关系, 地震地质, 28(4), 511-535。

倪四道 (2008), 应急地震学的研究进展, 中国科学院院刊, 23(4), 311-316。

杨智娴,张培震 (1998), 面波震级与体波震级,地方震震级间的经验关系及不确定性评价, 地震学报(5), 454-460。

Convers, J. A., and A. V. Newman (2013), Rapid earthquake rupture duration estimates from teleseismic energy rates, with application to real‐time warning, Geophys. Res. Lett., 40(22), 5844-5848.

Crotwell, H. P., T. J. Owens, and J. Ritsema (1999), The TauP Toolkit: Flexible seismic travel-time and ray-path utilities, Seismol. Res. Lett., 70(2), 154-160.

Duputel, Z., L. Rivera, H. Kanamori, and G. P. Hayes (2012), W phase source inversion for moderate to large earthquakes (1990–2010), Geophysical Journal International, 189(2), 1125-1147.

Duputel, Z., V. C. Tsai, L. Rivera, and H. Kanamori (2013), Using centroid time-delays to characterize source durations and identify earthquakes with unique characteristics, Earth and Planetary Science Letters, 374, 92-100.

Ekström, G., R. S. Stein, J. Eaton, and D. Eberhart‐Phillips (1992), Seismicity and geometry of a 110‐km‐long blind thrust fault 1. The 1985 Kettleman Hills, California, earthquake, Journal of Geophysical Research: Solid Earth (1978–2012), 97(B4), 4843-4864.

Fan, W., and P. M. Shearer (2015), Detailed rupture imaging of the 25 April 2015 Nepal earthquake using teleseismic P waves, Geophysical Research Letters, 42(14), 5744-5752.

Fan, W., and P. M. Shearer (2017), Investigation of Backprojection Uncertainties With M6 Earthquakes, Journal of Geophysical Research Solid Earth, 122(10), 5854.

Freymueller, J. T., H. Woodard, S. C. Cohen, R. Cross, J. Elliott, C. F. Larsen, S. Hreinsdóttir, and C. Zweck (2008), Active deformation processes in Alaska, based

on 15 years of GPS measurements, Geophys. Monogr. Ser., 179, 1-42, doi:10.1029/179GM02.

Fujii, Y., K. Satake, S. I. Sakai, M. Shinohara, and T. Kanazawa (2011), Tsunami source of the 2011 off the Pacific coast of Tohoku Earthquake, Earth Planets & Space, 63(7), 815-820.

Hamling, I. J., S. Hreinsdóttir, K. Clark, J. Elliott, C. Liang, E. Fielding, N. Litchfield, P. Villamor, L. Wallace, and T. J. Wright (2017), Complex multifault rupture during the 2016 Mw 7.8 Kaikōura earthquake, New Zealand, Science, 356(6334), eaam7194.

Hanks, T. C., and H. Kanamori (1979), A moment magnitude scale, Journal of Geophysical Research, 84, 2348-2350.

Hara, T. (2007), Measurement of the duration of high-frequency energy radiation and its application to determination of the magnitudes of large shallow earthquakes, Earth, Planets and Space, 59(4), 227-231.

Hara, T. (2008), Temporal characteristics of high band-pass filtered teleseismic P-waveforms from large shallow earthquakes, Earth, Planets and Space, 781-784 pp., doi:10.1186/BF03352827.

Hara, T. (2011), Magnitude determination using duration of high frequency energy radiation and displacement amplitude: application to the 2011 off the Pacific coast of Tohoku Earthquake, Earth, Planets and Space, 63(7), 3, doi:10.5047/eps.2011.05.014.

Hayes, G. P., P. S. Earle, H. M. Benz, D. J. Wald, and R. W. Briggs (2011), 88 Hours: The U.S. Geological Survey National Earthquake Information Center Response to the 11 March 2011 Mw 9.0 Tohoku Earthquake, Seismol. Res. Lett., 82(4), 481-493.

Honda, R., Y. Yukutake, H. Ito, M. Harada, T. Aketagawa, A. Yoshida, S. i. Sakai, S. Nakagawa, N. Hirata, and K. Obara (2011), A complex rupture image of the 2011 off the Pacific coast of Tohoku Earthquake revealed by the MeSO-net, Earth, Planets and Space, 63(7), 583-588.

Iii, W. C. P., and D. E. Hayes (1968), Sea‐floor spreading in the Gulf of Alaska, J. Geophys. Res., 73(20), 6571-6580.

Ishii, M., P. M. Shearer, H. Houston, and J. E. Vidale (2005), Extent, duration and speed of the 2004 Sumatra-Andaman earthquake imaged by the Hi-Net array, Nature, 435(7044), 933-936, doi:Doi 10.1038/Nature03675.

Kennett, B., and E. Engdahl (1991), Traveltimes for global earthquake location and phase identification, Geophys. J. Int., 105(2), 429-465.

Koper, K. D., A. R. Hutko, T. Lay, and O. Sufri (2012), Imaging short‐period seismic radiation from the 27 February 2010 Chile (MW 8.8) earthquake by back‐projection of P, PP, and PKIKP waves, J. Geophys. Res. B Solid Earth, 117(B2).

Krüger, F., and M. Ohrnberger (2005), Tracking the rupture of the M-w=9.3 Sumatra earthquake over 1,150 km at teleseismic distance, Nature, 435(7044), 937-939, doi:Doi 10.1038/Nature03696.

Meng, L., A. Inbal, and J. P. Ampuero (2011), A window into the complexity of the dynamic rupture of the 2011 Mw 9 Tohoku‐Oki earthquake, Geophysical Research Letters, 38(7), L00G07.

Mori, N., T. Takahashi, T. Yasuda, and H. Yanagisawa (2011), Survey of 2011 Tohoku earthquake tsunami inundation and run‐up, Geophys. Res. Lett., 38(7), 178-187.

Naugler, F. P., and J. M. Wageman (1973), Gulf of Alaska: Magnetic Anomalies, Fracture Zones, and Plate Interaction, Geol. Soc. Am. Bull., 84(5), 815-821.

Pavlis, G. L. (2003), "An Introduction to Seismology, Earthquakes, and Earth Structure" by Seth Stein and Michael Wysession, Seismological Research Letters, 74(6), 824-825.

Pegler, G., and S. Das (1996), THE 1987-1992 GULF OF ALASKA EARTHQUAKES, Tectonophysics, 257, 111-136.

Satriano, C., E. Kiraly, P. Bernard, and J. P. Vilotte (2012), The 2012 Mw 8.6 Sumatra earthquake: Evidence of westward sequential seismic ruptures associated to the reactivation of a N‐S ocean fabric, Geophysical Research Letters, 39(15), L15302.

Tsuboi, S., K. Abe, K. Takano, and Y. Yamanaka (1995), Rapid Determination of Mw from Broadband P Waveforms, Bull.seism.soc.am, 85(2), 606-613.

Wang, D., Y. Chen, Q. Wang, and J. Mori (2018), Complex rupture of the 13 November 2016 M w 7.8 Kaikoura, New Zealand earthquake: Comparison of high-frequency and low-frequency observations, Tectonophysics, 733, 100-107.

Wang, D., H. Kawakatsu, J. Mori, B. Ali, Z. Ren, and X. Shen (2016a), Backprojection analyses from four regional arrays for rupture over a curved dipping fault: The Mw 7.7 24 September 2013 Pakistan earthquake, Journal of Geophysical Research: Solid Earth, 121(3), 1948-1961.

Wang, D., H. Kawakatsu, J. Zhuang, J. Mori, T. Maeda, H. Tsuruoka, and X. Zhao (2017), Automated determination of magnitude and source length of large earthquakes using back projection and P wave amplitudes, Geophysical Research Letters, 44(11), doi:10.1002/2017GL073801.

Wang, D., and J. Mori (2016), Short-Period Energy of the 25 April 2015Mw 7.8 Nepal Earthquake Determined from Backprojection Using Four Arrays in Europe, China, Japan, and Australia, Bulletin of the Seismological Society of America, 106(1), 259-266.

Wang, D., N. Takeuchi, H. Kawakatsu, and J. Mori (2016b), Estimating high frequency energy radiation of large earthquakes by image deconvolution back-projection, Earth & Planetary Science Letters, 155-163 pp., doi:10.1016/j.epsl.2016.05.051.

Wells, D. L., and K. J. Coppersmith (1994), New empirical relationships among magnitude, rupture length, rupture width, rupture area, and surface displacement, Bull. Seismol. Soc. Am., 84(4), 974-1002.

Xiaoming Wang, and L. F. Liu (2006), An analysis of 2004 Sumatra earthquake fault plane mechanisms and Indian Ocean tsunami, Journal of Hydraulic Research, 44(2), 147-154.

Yagi, Y., and R. Okuwaki (2015), Integrated seismic source model of the 2015 Gorkha, Nepal, earthquake, Geophysical Research Letters, 42(15), 6229-6235.

Yao, H., P. M. Shearer, and P. Gerstoft (2013), Compressive sensing of frequency-dependent seismic radiation from subduction zone megathrust ruptures, Proc. Nat. Acad. Sci. U.S.A., 110(12), 4512-4517.

Zare, M., and S. Ghaychi Afrouz (2012), Crisis Management of Tohoku; Japan Earthquake and Tsunami, 11 March 2011, 12-20 pp.

Zhang, H., Z. Ge, and L. Ding (2011), Three sub-events composing the 2011 off the Pacific coast of Tohoku Earthquake (M w 9.0) inferred from rupture imaging by back-projecting teleseismic P waves, Earth, planets and space, 63(7), 595-598.

Zheng, X. F., Z. X. Yao, J. H. Liang, and J. Zheng (2010), The Role Played and Opportunities Provided by IGP DMC of China National Seismic Network in Wenchuan Earthquake Disaster Relief and Researches, Bull. Seismol. Soc. Am., 100(5), 2866-2872.